IEEE Access
Multidisciplinary | Rapid Review | Open Access Journal

Received August 4, 2018, accepted September 25, 2018, date of publication October 25, 2018,
date of current version November 30, 2018.

Digital Object Identifier 10.1109/ACCESS.2018.2876495

An Innovative Rail Pressure Sensor Signal Processing Algorithm to Determine the Start of Injection and End of Injection of Diesel Engines With Common Rail Injection Systems

QINMIAO KANG[1,2], YONG LI[3], (Senior Member, IEEE), ZHIFENG XIE[1], YONGQUAN LIU[2], AND MING ZHOU[1]

[1]School of Aerospace Engineering, Tsinghua University, Beijing 100084, China
[2]606 Institute, Chinese Aeronautical Establishment, Shenyang 110015, China
[3]Department of Electronic Engineering, Tsinghua University, Beijing 100084, China

Corresponding author: Zhifeng Xie (xzhf@tsinghua.edu.cn)

ABSTRACT This paper proposes an innovative rail pressure sensor signal processing algorithm to determine the start of injection and end of injection for single or multiple injections of diesel engines with a common rail injection system (CRIS). The importance of fuel injection timing (FIT) and fuel injection volume (FIV) in the CRIS is discussed, as well as the current progress of research in this field. The working principle of a solenoid valve injector is also described, pressure wave propagation is analyzed, and the characteristics of pressure waves are studied by simulation and experiments. The proposed algorithm has high reliability and flexibility and can be adjusted in real time according to engine operating status. The algorithm can effectively avoid the defects and shortcomings of traditional engine matching calibration, enhance the control precision of the FIT and FIV, improve the consistency and stability of fuel injection, and is expected to promote the performance of engine on fuel economy and pollutant emissions. The hardware implementation of this algorithm in practical ECU is also presented.

INDEX TERMS Signal processing algorithm, rail pressure sensor, start of injection, end of injection, diesel engine, CRIS.

I. INTRODUCTION

More stringent emission standards and rising fuel prices lead to increasing demand for diesel engines to be environmentally friendly and economical driving systems. Common rail injection systems (CRIS) are widely equipped with diesel engines. Flexible injection rules have been attained, including the customization of injection pressure, fuel injection pulse width, number of injections, and fuel injection volume (FIV). However, to ensure consistent and stable injection of different cylinders and cycles, fuel injection parameters should be closed-loop controlled and some literature, for example [1], [2], has presented research on this subject.

Fuel injection timing (FIT) and FIV have critical impact on engine performance, including dynamics and pollutant emissions [3]–[6]. However, due to the discreteness of the characteristic parameters of fuel injection system components, such as high-pressure fuel rail, fuel injectors, and high-pressure fuel delivery pipes, it is difficult to obtain the definite Start of Injection (SOI) and End of Injection (EOI) [7]. It is also almost impossible to calculate the actual FIT and FIV, together with the closed-loop control of the fuel injection advance angle, which has a huge impact on the power, economy, and pollutant emissions of the diesel engine. To achieve precise control of FIT, FIV and fuel injection advance angle, the traditional method is to obtain the dispersion of characteristic parameters of each component of the fuel injection system by means of engine matching calibration. However, this method has the drawback of large workload, long cycle, and the inability to perform precise closed-loop control.

There are three main ways to measure or calculate the SOI and EOI of a diesel engine. One way [8], [9] is to detect the injector drive current, though the accuracy is not high with this method. Another method [10]–[13] is to install sensor

on the injector, such as a needle closing sensor, though this will increase the injector design difficulty, and reduce the reliability of the injector. The third method [14], [15] is to drill holes in the cylinder and measure SOI and EOI, but the downside to this is that it will reduce the cylinder strength.

This paper proposes a rail pressure sensor signal processing algorithm to solve the problems in these calculation methods. The fuel injection of diesel engines is divided into pre-injection, main injection and post-injection. The main injection has the greatest impact on all aspects of the engine performance which is the reason this article focuses on this injection. It is proposed that the SOI and EOI are obtained by detecting the high-pressure fuel rail pressure change. This method can accurately obtain the SOI and EOI, then calculate the FIT and FIV. Therefore, closed-loop control of the injection advance angle and closed-loop compensation can both be carried out, effectively avoiding the various defects and deficiencies of the conventional methods.

This paper is organized as follows. In Section II, the system architecture and working principle of CRIS solenoid valve injector is introduced. In Section III, the fuel flow model is built and characteristics of pressure wave propagation are analyzed. The rail pressure signal processing algorithm to precisely calculate the SOI and EOI is presented in Section IV. In Section V, the effectiveness of the signal processing algorithm is verified through software simulation and practical engine testing. Finally, conclusions are drawn in Section VI.

II. WORK PRINCIPLE OF THE SOLENOID VALVE INJECTOR

A. ARCHITECTURE OF THE CRIS

A typical CRIS consists of a gear pump, a high-pressure pump, supply pipe, a high-pressure fuel rail, delivery pipes, an injector for each cylinder, sensors, actuators and an electronic engine control unit (ECU), as shown in Fig. 1. The high pressure pump driven by a crankshaft produces high pressure fuel, then squeezes the fuel into the supply pipe and high-pressure fuel rail. The high-pressure fuel rail with large volume capacity acts as a reservoir, connecting to the injector by high-pressure fuel delivery pipes. According to the engine operating status, ECU calculates the FIT and FIV, and they are controlled individually for each engine cylinder.

The gear pump lifts the fuel from the tank, via a filter, then the fuel is transferred to the high-pressure pump. The high-pressure pump generates pressure required for injection and the fuel is then transferred to the high-pressure fuel rail. Following this, the fuel runs through a high-pressure fuel delivery pipe to the injector and is injected into the combustion chamber at a pressure of 20∼270 MPa on the nozzle side [16], [17].

B. INJECTION TIMING

Sensors, actuators and ECU hardware systems related to fuel injection are shown in Fig. 2. The relationship between the fuel injection process and the above components is as follows.

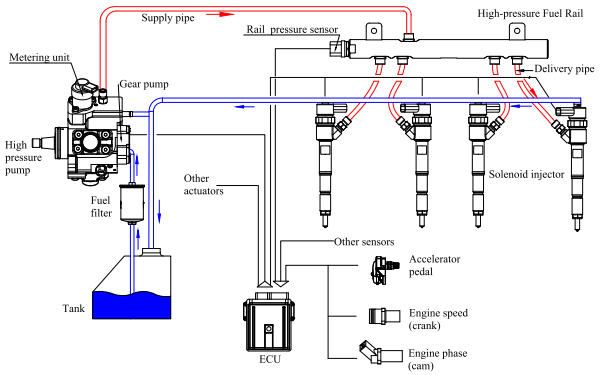

FIGURE 1. Architecture of a typical CRIS.

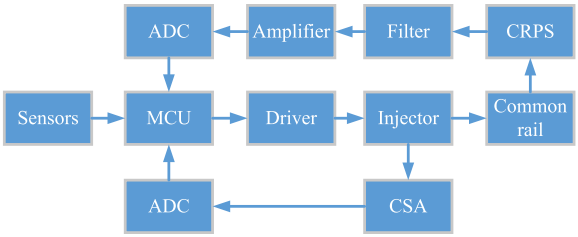

FIGURE 2. Sensors, actuators and ECU hardware systems related to fuel injection.

The micro controller unit (MCU) calculates FIT and FIV according to the engine operating status, then outputs the pulse width modulation (PWM) control signal. The driver receives the PWM control signal and improves the ability of the control signal to drive the injector solenoid valve actuator. The current sensing amplifier (CSA) detects the drive current of the solenoid valve and undertakes closed-loop control of the drive current through analog-to-digital (ADC) conversion, thus improving control accuracy of the solenoid valve. The common rail pressure sensor (CRPS) detects the rail pressure change and converts it into a voltage signal. After filtering and amplification, the rail pressure changes are converted to digital signals for MCU processing through ADC.

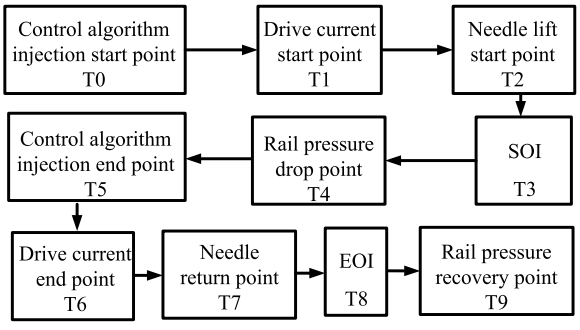

FIGURE 3. Typical FIT.

As is illustrated in Fig. 3, a typical FIT includes the following characteristic point: control algorithm injection start point T0, drive current start point T1, needle lift start point

T2, SOI T3, rail pressure drop point T4, control algorithm injection end point T5, drive current end point T6, needle return point T7, EOI T8, rail pressure recovery point T9.

To accurately obtain the SOI and EOI, T3 and T8 must be measured directly. The direct measurement of T3 and T8 must be carried out in the engine combustion chamber, however this is unsafe and unrealistic. Therefore, T3 and T8 are measured indirectly by the measurement of T4 and T9. The algorithm proposed in this paper is to determine the desired T3 from T4 and T4-T3 is the propagation time of the pressure wave from the needle to CRPS. Similarly, the desired T8 can be determined from T9 and T9-T8 is the propagation time of the pressure wave.

It is known that fuel injection and fuel supply from the pump will cause rail pressure fluctuations. To focus on the impact of fuel injection events on rail pressure fluctuations, the fuel supply should be set away from the fuel injection event. Such an arrangement is easy to implement in the engine because the fuel pump is driven by a timing belt or a timing chain.

C. WORKING STATES OF THE SOLENOID VALVE

The coupled relationship between drive circuit, electromagnetic force of the solenoid valve, and the dynamic model of the armature is displayed in Fig. 4. The model of electromagnetic force returns $\lambda = N\phi$ to the model of drive circuit, obtaining the peak current I of the next simulation step from the circuit submodule, outputting the electromagnetic force F_m to the dynamic model, and obtaining the armature displacement δ from the dynamic model to calculate the air gap reluctance.

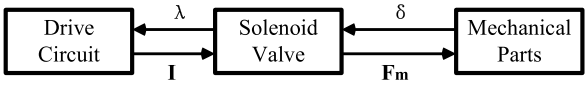

FIGURE 4. Coupled relation between drive circuit, electromagnetic force of the solenoid valve and the armature dynamic model.

The following two subsections will describe the working mode and drive circuit of the solenoid valve as both have a large influence on fuel injection characteristics [18]. A typical common rail injector includes solenoid valves, as well as a control chamber, valve control plunger, needle, springs and nozzles. An outline of this structure is presented in Fig. 5. The common rail injector is a very complex and precise submodule in CRIS.

The four main working states of the solenoid valve are outlined below. The convention adopted is that when the solenoid valve is in open state, the armature is far away from solenoid, and the ball valve contacts with its seat, no fuel injection occurs.

1) Closing process
The solenoid valve is in the open state when there is no drive current. When the fuel injection control signal is sent by MCU, the drive circuit applies the peak drive current to both ends of the solenoid valve.

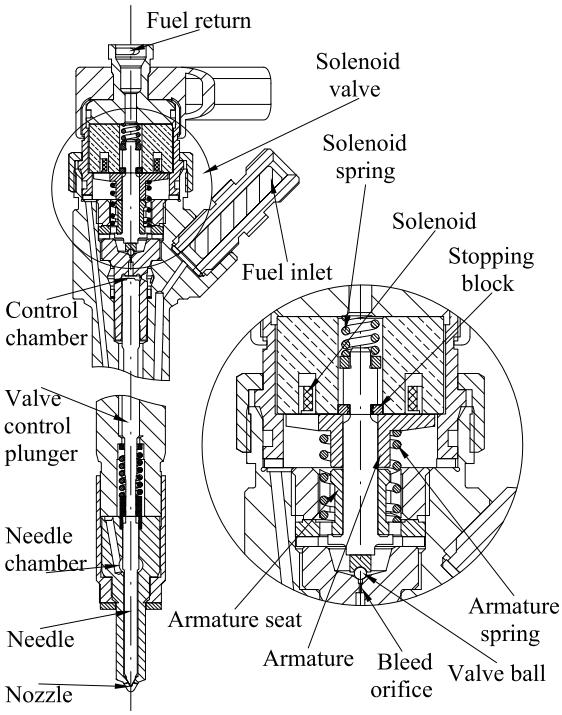

FIGURE 5. Structure of a typical common rail injector and the solenoid valve.

Under the action of drive current, the electromagnet creates a magnetic field and produces electromagnetic force acting on the armature. When the electromagnetic force is greater than the initial movement resistance, the armature will move together and close the solenoid valve. When the armature is seated for the first time, it collides with the armature seat and rebounds. Under the action of electromagnetic force, the armature continues to rebound and finally to seat. In the continuous rebound process, the kinetic energy of the armature is consumed by the collision process and hydraulic damping, and eventually is seated and no longer rebounds, entering a stable closed state.

2) Stable closed state
When the solenoid valve is closed, the air gap is very small, reluctance decreases, and the magnetic flux and electromagnetic force increases. At this time, a smaller drive current can provide sufficient electromagnetic force to maintain the closed state of the solenoid valve, which can reduce power consumption of the system while ensuring the reliable closure of the solenoid valve. To achieve fuel injection, the solenoid valve closes, the fuel bleed orifice is closed and the fuel pressure in the control chamber drops sharply, then the hydraulic pressure from control chamber on valve control plunger and needle will drop and it will move, then the needle lifts and fuel injection begins.

3) Opening process
When the control pulse terminates, the drive current in the solenoid valve drastically decreases and the

electromagnetic force decreases rapidly too. The armature will move to the direction of the air gap under the action of hydraulic force and springs force, and the solenoid valve will open. Like the closing process, the armature will rebound when it contacts the stopping block.

4) Stable opened state
After the rebound process, the solenoid valve is in stable opened state and the ball valve is closed and the control plunger and needle will move down under the action of hydraulic force and springs force, then the needle valve is in stable closed state.

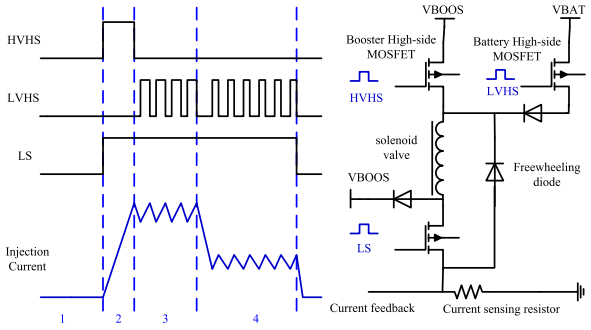

FIGURE 6. Drive principle and drive circuit of the solenoid valve.

D. DRIVE PRINCIPLE AND DRIVE CIRCUIT OF THE SOLENOID VALVE

The drive principle and drive circuit of the solenoid valve is displayed in Fig. 6. There are four different solenoid valve drive phases for each fuel injection, which are described as follows.

1) Booster phase (the second phase in Fig. 6
The low side metal-oxide-semiconductor field-effect transistor (MOSFET) and the booster high-side MOSFET are opened simultaneously. Voltage of the solenoid valve is up to VBOOS, and the drive current of the electromagnet rises rapidly until the target peak current Ip is reached.
2) Large current modulation phase (the third phase in Fig. 6)
ECU detects the drive current of the solenoid valve via the current sensing circuit. When drive current reaches the target peak Ip, it closes the booster high-side MOSFET and enters the current feedback control phase. At this time, while the booster high-side MOSFET is closed, the battery high-side MOSFET performs substantial current modulation with a higher PWM duty cycle. This phase corresponds to the closing process of the solenoid valve.
3) Holding current modulation phase (the fourth phase in Fig. 6)
At this phase, the solenoid valve has been completely closed. Only a small drive current is needed to maintain the closed state and the battery high-side MOSFET uses a small PWM duty cycle to carry out holding current modulation.
4) End of injection phase
At the end of the fuel injection, the battery high-side MOSFET and the low side MOSFET are turned off simultaneously. The instantaneous induction voltage of the solenoid valve breaks through the internal avalanche diode parallel to the MOSFET and forms a discharge circuit through a freewheeling diode.
Battery voltage is supplied by the vehicle battery, and has low internal resistance and high output current. The VBOOS voltage is obtained through the DC/DC boost converter and the voltage on the output capacitor of the DC/DC booster can be closed-loop controlled by the voltage detection circuit.

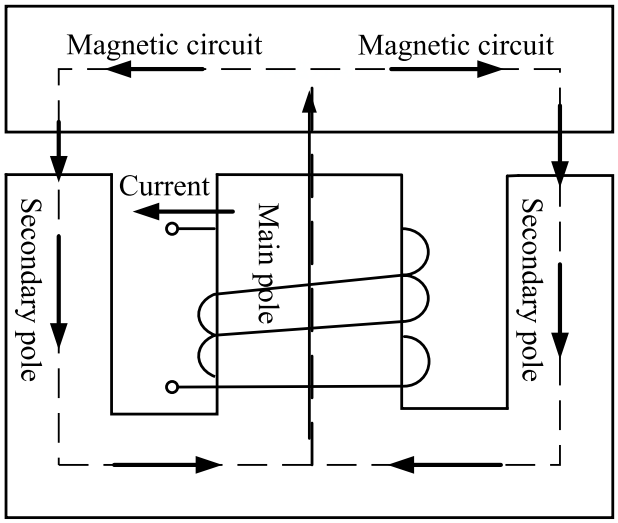

FIGURE 7. Magnetic circuit of the solenoid valve electromagnet and armature.

E. ELECTROMAGNETIC FORCE OF THE SOLENOID VALVE

The magnetic circuit of the solenoid valve electromagnet and armature is shown in Fig. 7. There is a flux leakage between the main pole and the secondary pole. For armature, the air gap between each pole and armature is equivalent to a magnetic resistance according to the uniform magnetic field theory. The influence of the edge magnetic field is taken into account by the correction coefficient and the influence of small damping orifice is neglected. For the non-working air gap, each air gap is also equivalent to a magnetic flux leakage magnetic resistance, but the magnetic saturation of the coil is caused by the solenoid valve in the closing process. The magnetic potential drop along the pole cannot be ignored, so the magnetic potential added at both ends of the magnetic flux magnetic resistance needs to take the equivalent magnetic potential of the whole air gap into account. Since the leakage flux is very small relative to the total magnetic flux, the effect of magnetic flux on the distribution of magnetic potential can

be ignored. The distribution of magnetic potential along the pole column is linear, so the magnetic potential of the middle point in the non-working air gap is taken as the equivalent air gap magnetic potential drop.

The electromagnetic force can be calculated as follows. According to the Ampere loop theorem and Kirchhoff's second law of magnetic path, the equivalent magnetic circuit of the solenoid valve is expressed in Eq.1

$$\frac{1}{2}I \cdot N = \sum_j H_j l_j \tag{1}$$

where j is the sequence number of magnetic circuit, and l_j is the length of magnetic circuit.

Considering the flux continuity theorem, produces,

$$H = \mu(B) \cdot B, \ \phi_{core} = \phi_{arm} + \phi_{leakage} \tag{2}$$

In accordance with Ohm's law used in magnetic circuits and the definition of magnetic flux, provides:

$$\phi_j = B_j \cdot A_j = \frac{H_j}{R_{mj}} \tag{3}$$

where A_j is the cross sections of the magnetic circuit, R_{mj} is magnetic resistance including leaked magnetic resistance. For uniform cross sections of the magnetic circuit, R_{mj} can be found,

$$R_{mj} = \frac{l_j}{\mu_j A_j} \tag{4}$$

Electromagnetic force F_m can be written as

$$F_m = \frac{2}{\mu_0}\left(\frac{\phi_{arm}^2}{2A_5} + \frac{\phi_{arm}^2}{2A_3}\right) \tag{5}$$

F. DYNAMIC MODEL OF THE ARMATURE

As described in Subsection II-E, the expression of electromagnetic force F_m of the armature is obtained. Gravitational force, springs force and damping force also act on the armature along with electromagnetic force. The equation of motion for armature and valve can be written as:

$$m\,\ddot{\delta} + F_m + F_f + F_{spr} + F_b = 0 \tag{6}$$

where m is the mass of armature and valve, δ is the displacement of armature with valve, F_f is the total damping force, F_{spr} is springs force, and F_b is the contact force between armature and its site.

Using the elastic collision model, provides:

$$F_b = \begin{cases} k_{bmax}(\delta - \delta_{max}) \\ \quad + C_{bmax}(1 - e^{\frac{-3\delta}{kemax}})\dot{\delta}, & \delta > \delta_{max} \\ k_{bmin}(\delta - \delta_{min}) \\ \quad + C_{bmin}(1 - e^{\frac{-3\delta}{kemin}})\dot{\delta}, & \delta < \delta_{min} \\ 0, & \delta_{min} < \delta \le \delta_{max} \end{cases} \tag{7}$$

where k_{bmax} is the contact stiffness between the armature and stopping block and C_{bmax} is the friction coefficient between the armature and stopping block, as displayed in Fig. 8.

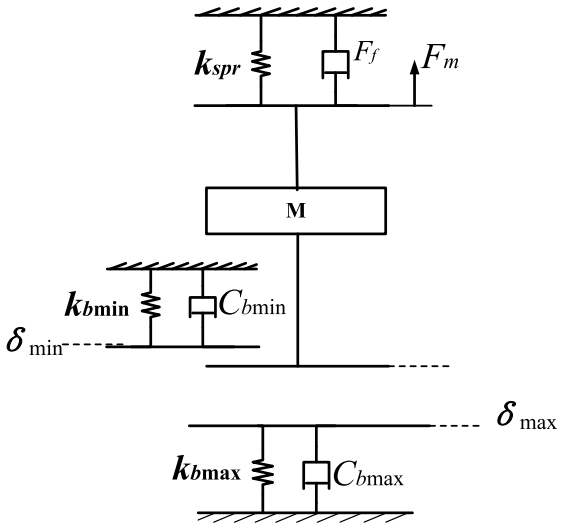

FIGURE 8. Dynamic model of the solenoid valve.

An empirical relation is $C_{bmax} = 0.06 \cdot \sqrt{k_{bmax} \cdot m}$. The contact stiffness between the armature and armature seat is k_{emax}, and C_{emax} is the corresponding friction coefficient. The transition distances between the armature and stopping block is k_{emax} and k_{emin} is the armature seat in this circumstance.

The total damping force is:

$$F_f = F_{fric} \cdot sign(\dot{\delta}) + F_{wind} + F_{visc} \tag{8}$$

where F_{fric}, F_{visc}, *and* F_{wind} can be written as

$$\begin{aligned} F_f &= F_{dyn} + (F_{stat} - F_{dyn})e^{\frac{-3|\dot{\delta}|}{V_0}} \\ F_{visc} &= R_{visc}\dot{\delta} \\ F_{wind} &= R_{wind}\dot{\delta}|\dot{\delta}|, \end{aligned} \tag{9}$$

where F_{dyn} is dynamic friction force and F_{stat} is static friction force, V_0 is the critical speed value when the static friction changes into dynamic friction, R_{visc} is the coefficient of viscosity and $R_{wind} \approx 200N/(m/s)^2$ is the drag coefficient of fuel.

The total springs force is:

$$F_{spr} = \sum_{i=1}^{2} k_{spr,i} \cdot (h_i + \delta_{max} - \delta) \tag{10}$$

where $i = 1$ and 2 is indicated for solenoid spring and armature spring, respectively. h_i and $k_{spr,i}$ are the precompressed length, stiffness of spring i, respectively.

III. CALCULATION THE PROPAGATION TIME OF PRESSURE WAVE

Research has shown that pressure wave characteristics in the CRIS can be used for the diagnosis of injection events [19], the determination of the duration of injection [20], and other factors. This paper will develop an algorithm to obtain the exact SOI and EOI from the rail pressure signal. As introduced in section II B, to obtain accurate SOI and EOI, the time

of pressure wave propagation must be calculated precisely. This begins with the pressure wave propagation equation in the high pressure hydraulic circuit.

The high pressure hydraulic circuit in CRIS can be divided into two categories, which have different flow models. One is chamber, such as the delivery chamber and the control chamber in the injector. The other is thin tube, including the delivery pipe and the fuel passage with a smaller radius inside the injector.

A. FLOW EQUATION IN CHAMBERS

In the hydraulic circuit, pressure and velocity distribution should be uniform. With reference to any chamber j in the mathematical model, the continuity equation is:

$$\dot{q}_{in,j} - \dot{q}_{out,j} = \frac{V_j}{\beta}\frac{dp_j}{dt} + \frac{dV_j}{dt} \tag{11}$$

where $\dot{q}_{in,j}$ and $\dot{q}_{out,j}$ are the volume flow rates of coming into and going out of the chamber j, respectively, V_j is the chamber volume, p_j is the pressure in the chamber, and β is the bulk modulus of the fuel.

B. FLOW EQUATION IN PIPE

When the drive current in the solenoid valve is large enough, the armature with the sphere valve will move under electromagnetic force, then the needle will move and fuel injection begins. Simultaneously, an expansion wave will be formed in the delivery chamber and the wave will propagate to the high-pressure fuel rail. When the needle closes, a compression wave will form and propagate to the high-pressure fuel rail. The phenomenon of generation and propagation of the pressure wave is similar to the water hammer, which can be simulated [21], [22] by solving the partial differential equation 12. Studies [23]–[25] have shown that one-dimensional equations can take into account the requirements of solution accuracy and computation time.

$$\begin{aligned} \frac{\partial p}{\partial t} + \frac{c_s^2}{A_{cr}}\frac{\partial q}{\partial x} &= 0 \\ \frac{1}{A_{cr}}\frac{\partial q}{\partial t} + \frac{\partial p}{\partial x} + 2f\frac{q|q|}{\rho D A_{cr}^2} &= 0 \end{aligned} \tag{12}$$

Where D is the diameter of the pipe, A_{cr} is the area of cross section of the pipe, c_s is the sound velocity $c_s = \sqrt{\beta/\rho/(1+K\beta)}$, K is the stiffness of the rail, ρ is the density of the fuel, and f is the Fanning friction factor [26]. If there is an injector $\gamma_i = 1$, otherwise $\gamma_i = 0$. A finite difference scheme is applied to transform the equation 12 into a set of ordinary differential equations.

$$\begin{aligned} q(0,t) = 0, \quad q(N,t) &= 0 \\ \frac{\partial q_i}{\partial x} &= \frac{1}{\Delta x}\left(q_{i+1} - q_i + \gamma_i q_{inj}\right) \\ \frac{\partial p_i}{\partial x} &= \frac{p_{i+1} - qi}{\Delta x} \end{aligned} \tag{13}$$

where $p_i(t)$, $q_i(t)$ are the pressure and volume flow rate of the ith cell, respectively, thus providing

$$\begin{aligned} q(0,t) = 0, \quad q(N,t) &= 0 \\ \frac{\partial q_i}{\partial x} &= \frac{1}{\Delta x}\left(q_{i+1} - q_i + \gamma_i q_{inj}\right) \\ \frac{\partial p_i}{\partial x} &= \frac{p_{i+1} - qi}{\Delta x} \end{aligned} \tag{14}$$

Consequently, the ordinary differential equation for ith element can be written as:

$$\begin{aligned} \frac{p_i(t+1) - p_i(t)}{\Delta t} &= \frac{C_s^2}{A_{cr}\Delta x}\left(q_i - q_{i+1} - \gamma_i q_{inj}\right) \\ \frac{q_i(t+1) - q_i(t)}{\Delta t} &= \frac{A_{cr}}{\Delta x}(p_i - p_{i+1}) - \frac{2f}{A_{cr}D\rho}q_i|q_i| \end{aligned} \tag{15}$$

where volume flow rate of the injector can be written as

$$q_{inj} = C_d A_i \sqrt{2\rho|p_i(t) - p|} \tag{16}$$

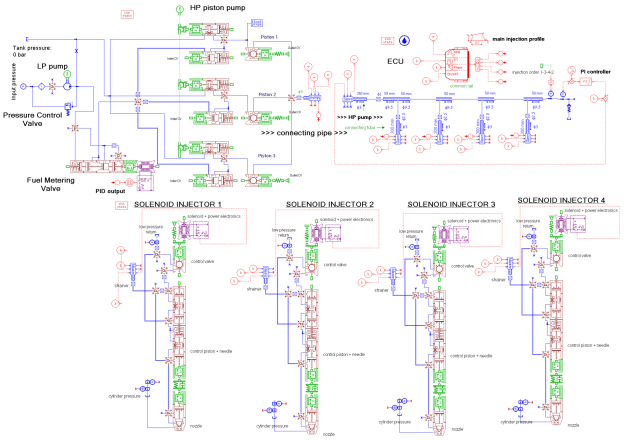

FIGURE 9. Dynamic model of the solenoid valve.

C. SIMULATION

The mathematical model of pressure wave built in the last subsection can be simulated in the widely used physics based commercial software AMEsim. The model for the low pressure and high pressure pump, high pressure fuel rail, and injector of CRIS are displayed in Fig. 9. The CRIS is equipped on a RA420 SOHC designed by VM Motori S.p.A., the key parameters of the engine are presented in Table 1. The main parameters of the model are outlined Table 2, and the layout of the fuel rail, supply pipe, delivery pipes and injector are presented in Fig. 10.

The propagation time of the pressure wave from the nozzle to the rail pressure sensor was examined in this study. Fig. 11 shows the rail pressure curve with its differential, and the needle lift when the target pressure is 150 MPa, speed is 3000 rpm and brake torque is 254 N· m. The time difference $\delta t = 0.28$ ms can be measured from the two vertical lines.

According to the fuel sound velocity formula, the sound velocity is approximately 1500 m/s [27]–[29], the fuel pipe

TABLE 1. The key parameters of RA420 SOHC.

Parameter	Value
Configuration	Inline four
Displacement	2.0 L
Cylinder bore	83.0 mm
Piston stroke	92.0 mm
Valvetrain	SOHC
Compression ratio	15.5:1
Power	110 kW@ 4000 rpm
Torque	300 N·m@ 2000 rpm
Turbocharger	Honeywell VGT
Fuel system	Bosch CRIS

TABLE 2. Key parameters of pressure wave propagation paths caused by fuel injection in CRIS.

Parameter	Value
Diameter of delivery pipe	3.0 mm
Diameter of high pressure fuel rail	9.5 mm
Volume of control chamber	20 mm^3
Volume of delivery chamber	200 mm^3

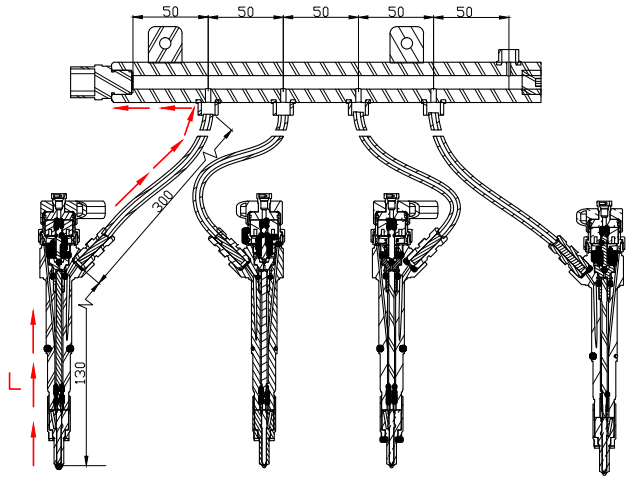

FIGURE 10. Layout of the high pressure fuel rail, high pressure fuel delivery pipes and injector of the CRIS.

length L, as shown in Fig. 10, is about 480 mm, so the pressure wave propagation time is approximately 0.32 ms. This is about 12% margin of error from the simulated results.

TABLE 3. Propagation time for different length of delivery pipe when the target pressure is 150 MPa, engine speed is 2000 rpm, brake torque is 120 N· m.

Length of delivery pipe/m	0.2	0.4	0.6
Time/ms	0.23	0.35	0.50

The effect of different delivery pipe lengths on pressure wave propagation was also examined. Table 3 shows the propagation time between the nozzle and rail pressure sensor when

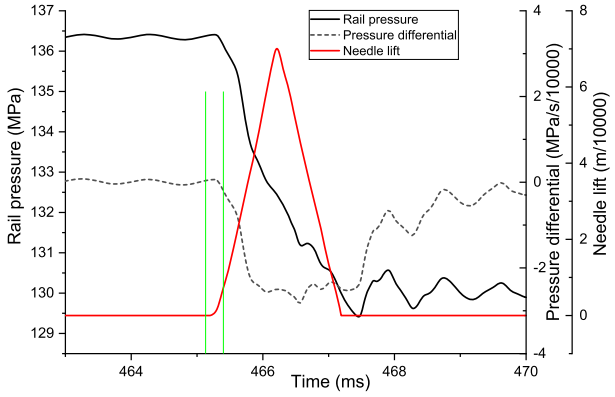

FIGURE 11. Rail pressure sensor signal and needle lift when the target pressure is 150 MPa, speed is 3000 rpm and brake torque is 254 N· m.

the target pressure is 150 MPa, engine speed is 2000 rpm, brake torque is 120 N· m and the length of delivery pipe is 0.2 m, 0.4 m and 0.6 m, respectively. From Table 3, we can conclude that the length of the fuel supply pipe has a significant influence on the propagation time of the pressure wave.

TABLE 4. Propagation time for different target rail pressures when the length of the fuel supply pipe is 0.3 m and engine speed is 2000 rpm.

Target rail pressure/MPa	100	150	180
Time/ms	0.27	0.28	0.28

The effects of different target rail pressures on the propagation time were also investigated. Table 4 presents the propagation time when the length of the fuel supply pipe is 0.3 m, engine speed is 2000 rpm with different target pressure and brake torque. From the Table 4 we can conclude that the influence of the target pressure on the pressure wave propagation time is almost negligible.

IV. RAIL PRESSURE SENSOR SIGNAL PROCESSING

According to the analysis in Section III, the propagation time of the pressure wave has almost no influence on engine operating status including engine speed and fuel rail pressure and is mainly determined by the length of the pressure wave propagation path. Therefore, for an engine product with CRIS, the propagation time of pressure waves from the injector nozzle to the rail pressure sensor is basically fixed. Analysis in Section II illustrates it is difficult to directly measure the actual SOI T3 and EOI T8. Therefore, the SOI and EOI are indirectly measured by direct measurement of the high-pressure fuel rail pressure dropping point T4 and the high-pressure fuel rail pressure recovery point T9, and then subtracting the pressure wave propagation time. In order to reduce the use of MCU computing resources and improve detection accuracy of SOI and EOI, the signal processing algorithm only begins running after the fuel injection control algorithm triggers the injection. When the SOI and EOI detection is completed, the algorithm stops running.

As illustrated in Fig. 3, the SOI and EOI of the fuel injection can be measured using the pressure wave in the fuel rail, which provides a relatively small error. The timing difference between the start point of the fuel injection control algorithm T0 and the injector drive current T1, the end point of the fuel injection control algorithm T5 and the end point of the injector drive current T6 is caused by the characteristics of the MCU and the injector drive circuit. The timing difference between the drive current starting point T1 and the fuel injection starting point T3, the drive current end point T6 and the fuel injection end point T8 is mainly determined by characteristics of the injector. Fuel pressure has little effect on this timing difference.

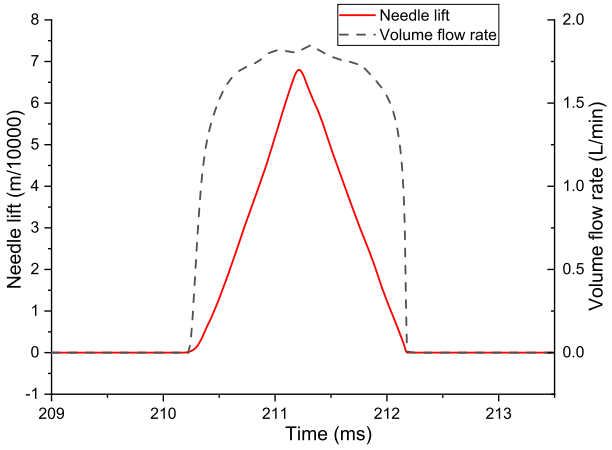

FIGURE 12. Needle lift and injector volume flow rate.

Fuel injection can cause the solenoid valve injector needle lift, as shown in Fig. 12. The pressure of the high-pressure fuel rail will fluctuate with the needle lift, as illustrated in Fig. 13. The pressure wave will propagate along the high-pressure fuel delivery pipe to the high-pressure fuel rail and can be detected by the rail pressure sensor which then converts the pressure signal into a voltage signal.

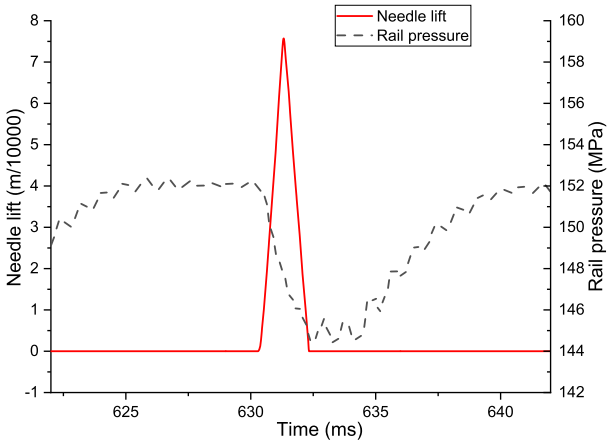

FIGURE 13. Needle lift and high-pressure fuel rail pressure.

The relationship between the fuel injection rate and the high-pressure fuel rail pressure fluctuation is displayed

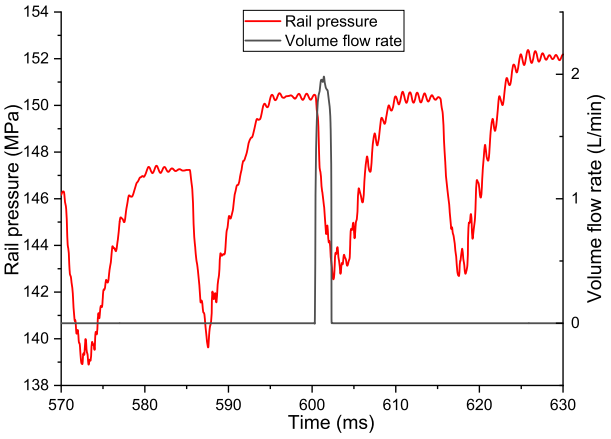

FIGURE 14. The relationship between the fuel injection rate and the high-pressure fuel rail pressure fluctuation.

in Fig. 14. It can be seen that the pressure in the high-pressure fuel rail will drastically decrease after fuel injection. This fuel rail pressure change value is in the range of 5∼10 MPa with the change of FIV. The voltage change of the rail pressure sensor is around 150∼300 mV.

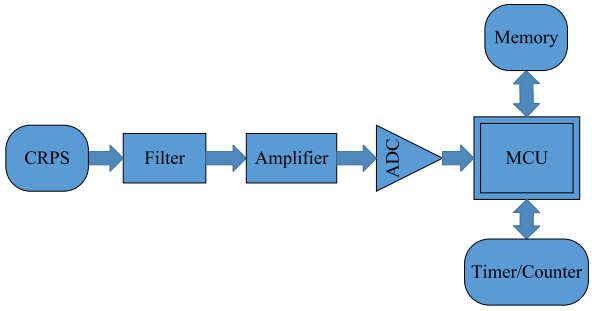

FIGURE 15. ECU hardware related to the rail pressure sensor signal processing.

ECU hardware related to rail pressure sensor signal processing is shown in Fig. 15. To ensure the rail pressure signal processing algorithm can be applied to the actual engine, the CRPS signal needs to be amplified and filtered, then converted to digital signal. Memory is also required to store relevant data, timer/counter records and to capture the corresponding time of SOI and EOI.

This study will introduce two signal processing algorithms for detecting SOI and EOI. The first algorithm establishes the control parameter MAPs, comparing the actual rail pressure changes with rail pressure changes caused by fuel injection under certain engine operating conditions. The second algorithm determines the SOI and EOI by detecting the rail pressure change rate, and has strong flexibility.

For the first signal processing algorithm, engine operating conditions are based on signals detected by sensors of the ECU, such as fuel temperature, rail pressure, coolant temperature, engine speed and phase.

A software flow chart of the first rail pressure sensor signal processing algorithm is presented in Fig. 16. To accurately

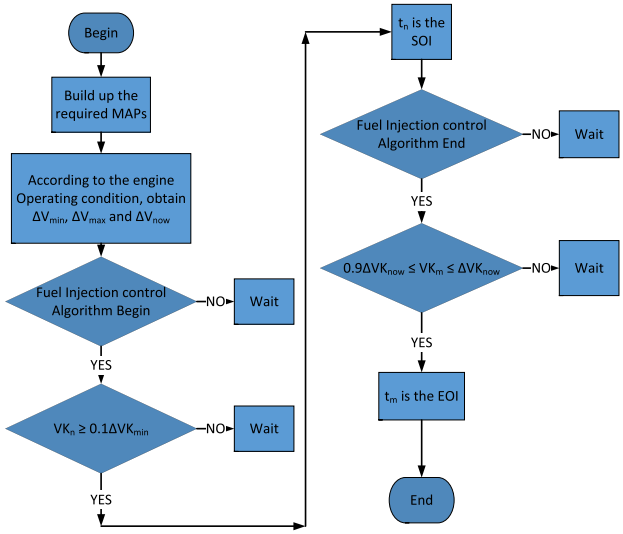

FIGURE 16. Software flow chart of the first kind rail pressure sensor signal processing algorithm.

detect the SOI and EOI through the change of rail pressure signal, three engine control MAPs must be established. These are the MAP of engine operating status and FIV, MAP of FIV and the high-pressure fuel rail pressure change, and MAP of the high-pressure fuel rail pressure change and voltage change of the rail pressure sensor. The MAP is an engine control array, reflecting the control parameters obtained by querying an array under a certain working condition. It can be one-dimensional, two-dimensional or even three-dimensional.

According to the MAP of engine operating status and FIV, the minimum FIV IV_{min}, the maximum FIV IV_{max} and the current FIV IV_{now} (including pre-injection, main-injection and post-injection) under the current engine operating status can be obtained. By the MAP of FIV and the high-pressure fuel rail pressure change, IV_{min}, IV_{max} and IV_{now} can be converted to the minimum high-pressure fuel rail pressure change ΔP_{min}, the maximum high-pressure fuel rail pressure change ΔP_{max}, and the current high-pressure fuel rail pressure change ΔP_{now}. Through the MAP of the high-pressure fuel rail pressure change and voltage change of the rail pressure sensor, the ΔP_{min}, ΔP_{max} and ΔP_{now} can be converted to the minimum voltage change ΔV_{min}, the maximum voltage change ΔV_{max} and the current voltage change ΔV_{now} of the rail pressure sensor under current engine operating status. In order to facilitate MCU to complete data processing, the above three analog variables ΔV_{min}, ΔV_{max} and ΔV_{now} must be converted to digital variables ΔVK_{min}, ΔVK_{max} and ΔVK_{now} through ADC.

It is assumed that at the fuel injection control algorithm starting point $T0$, the corresponding digital value of the rail pressure after the ADC conversion is VK_{T0}. Similarly, the corresponding digital value of the rail pressure at Tn after the ADC conversion is VK_{Tn}. The time for ADC to perform the Nth analog to digital conversion is Tn. As fuel injection occurs, the rail pressure will drop, so $VK_{Tn} < VK_{T0}$. Let VK_n be the rail pressure difference between $T0$ and Tn, which yields $VK_n = VK_{T0} - VK_{Tn}$.

According to the above analysis, the ΔVK_{min}, ΔVK_{max} and ΔVK_{now} of the current engine working status can be obtained. When the fuel injection control algorithm starts running, if $VK_n \geq 0.1\Delta VK_{min}$, it can be assumed that Tn is the SOI. When the fuel injection control algorithm is finished, if $0.9\Delta VK_{now} \leq VK_m \leq \Delta VK_{now}$, it can be understood that Tm is the EOI. 0.1 and 0.9 can be other suitable values, which need to be adjusted according to the design parameters of the engine fuel injection system.

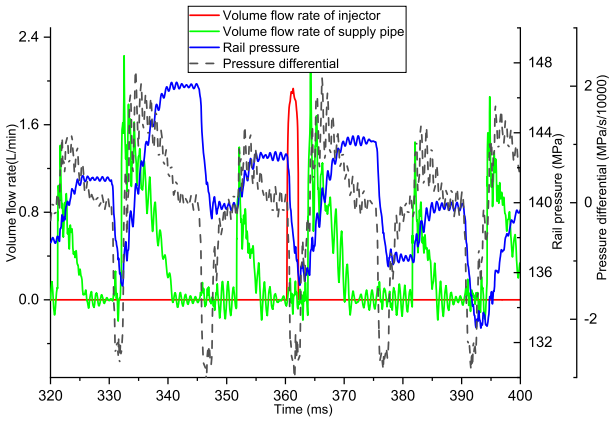

FIGURE 17. Volume flow rate of injector and high-pressure pump, fuel rail pressure and its change rate.

The fuel injection rate, fuel supply rate, fuel rail pressure, and its change rate during fuel injection for the second type of signal processing algorithm are shown in Fig. 17. It can be seen that when fuel injection occurs, the rail pressure will decrease significantly and the decrease rate is large. Once the fuel injection ends, the rail pressure will gradually stabilize to a certain value and recover to the target rail pressure.

The software flow chart of the second kind of rail pressure sensor signal processing algorithm is presented in Fig. 18. When fuel injection occurs, the change rate of the rail pressure illustrates that the time from near zero to the negative value is when fuel injection starts as the rail pressure change rate is negative. When there is a positive value, the fuel injection has ended. After this, positive and negative values will appear alternately as fuel injection will cause the rail pressure to oscillate, resulting in the rail pressure change rate fluctuating between positive and negative values. As the sampling frequency and conversion time of the ADC are fixed, there is no need for a division. The ADC converted rail pressure change can be obtained by comparing the rail pressure values of the two adjacent ADC conversions. The fuel injection control algorithm triggers the fuel injection time which is T0. When the counter begins, the ADC starts to convert the rail pressure sensor signal into a digital signal and stores it. When the ADC converted rail pressure change rate shows a negative value, it can be considered as the SOI (T3).

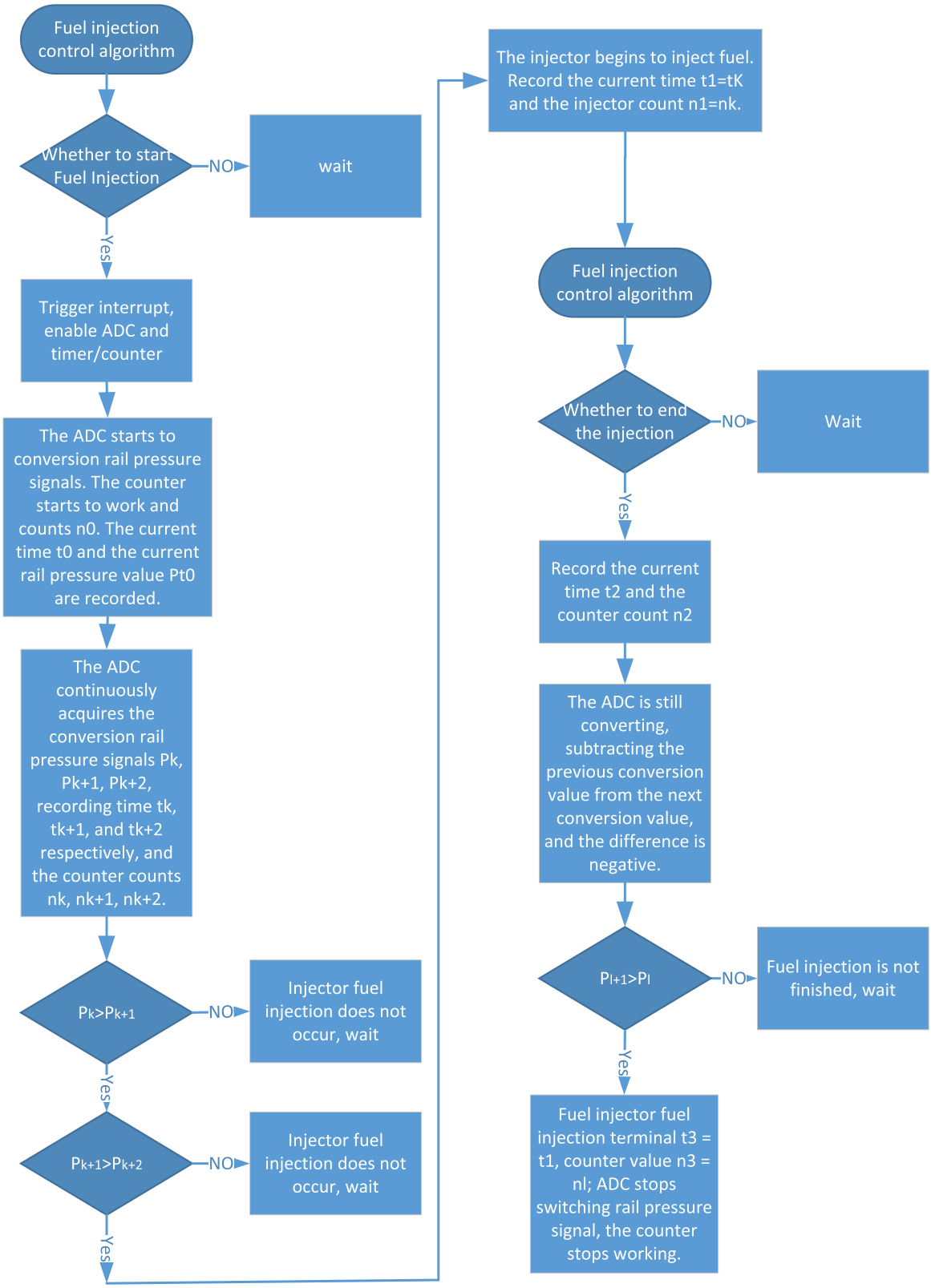

FIGURE 18. Software flow chart of the second kind rail pressure sensor signal processing algorithm.

For a certain number of consecutive comparisons, such as three, if the ADC converted rail pressure change rate is always a negative value, the time at which the first ADC converted data corresponds can be assumed to be SOI (T3).

Similarly, the fuel injection control algorithm triggers the end of fuel injection at time T5. After T5, when the ADC converted rail pressure change rate is positive for a period of time, and a positive value abruptly appears at a particular moment, this moment can be treated as the EOI (T8).

This section introduces two algorithms for determining SOI and EOI based on rail pressure sensor signals. In practical applications, one of these algorithms can be used separately, and the two algorithms can be combined to determine SOI and EOI more accurately.

The calculating method of the FIV is outlined as follows: the rail pressure before and after fuel injection is measured, and are P_1 and P_2, respectively. Volume V of the high pressure fuel rail is known. Literature [28], [29] shows the relationship between the fuel density ρ, the pressure P, $\rho = \rho(P)$, and the FIV is $\Delta m = V(\rho(P1) - \rho(P2))$. The above calculation can also take into account the temperature effect by introducing $\rho = \rho(P, T)$, where T is the fuel temperature.

V. VALIDATION

Engine parameters for the experiment are shown in Table 1. Three typical crankshaft speeds are selected, outlined in Table 5, which are the engine idle condition speed of 800 rpm, the speed where engine has maximum torque of 2000 rpm, and the common-used operation speed of 3000 rpm. To ensure the credibility of the experimental results, we selected the three speed cases for experiments. The rail pressure acquisition begins only after the engine is running stably. The acquisition was performed three times for each case. We find that these rail pressure data have the same variation characteristics. So we will take one of them for illustration.

TABLE 5. The main parameters set in simulation and experiment.

	case 1	case 2	case 3
speed/rpm	800	2000	3000
Target pressure/MPa	41.0	71.5	91.5

The experiment in this study was carried out on the RA420 SOHC. The testing engine and experiment environment is illustrated in Fig. 19. The engine was monitored by FreeMASTER, a user friendly real time debug monitor and data visualization tool. The rail pressure data can be drawn from the FreeMASTER database.

The simulation result of rail pressure for the three cases are displayed in Fig. 20, Fig. 21, Fig. 22, respectively. The sampling frequency of the data is 100 kHz.

The experimental result of rail pressure for the three cases are displayed in Fig. 23, Fig. 24, Fig. 25. The sampling frequency of this data is 300 Hz.

From the comparison of the above simulation and experimental results it can be seen that the change trend of the rail pressure between adjacent injections is essentially the same, being that when fuel injection starts, the rail pressure will decrease and after the injection, the rail pressure will return to a stable value. Due to changes in the external environment, the accuracy of the rail pressure control algorithm and the stable rail pressure after multiple injections may be different, but this does not affect the determination of SOI and EOI. Additionally, the sampling frequency of the rail pressure signal in

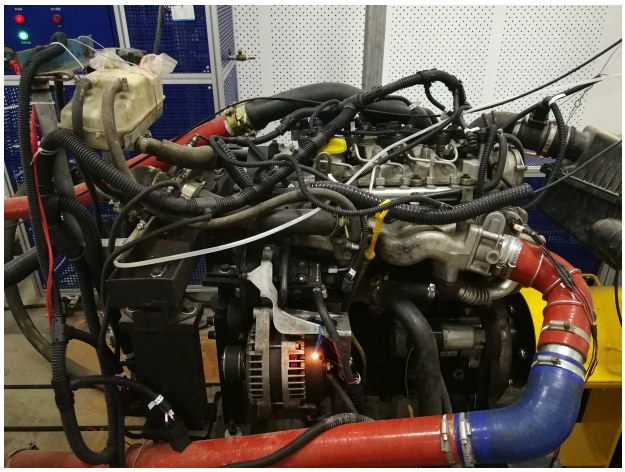

FIGURE 19. Testing engine and experiment environment.

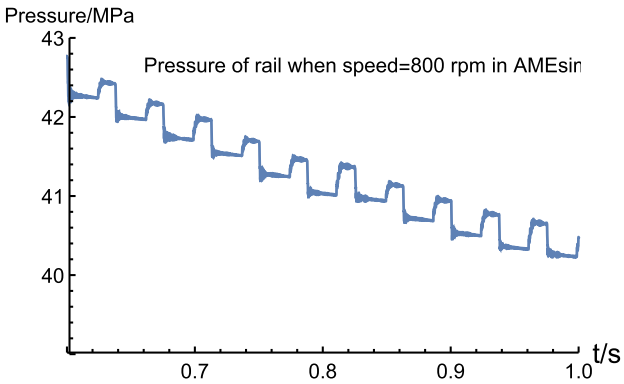

FIGURE 20. Simulation result of rail pressure when speed=800 rpm and brake torque=0.

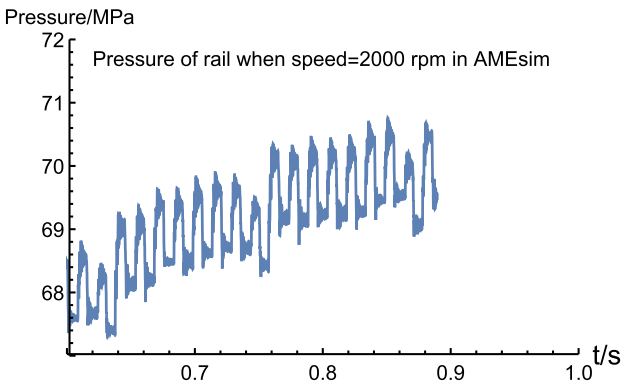

FIGURE 21. Simulation result of rail pressure when speed=2000 rpm and brake torque=0.

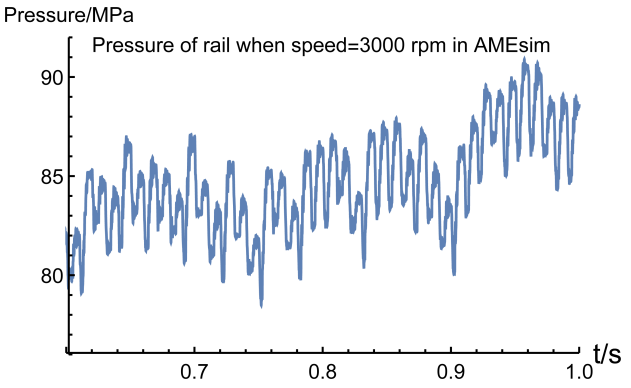

FIGURE 22. Simulation result of rail pressure when speed=3000 rpm and brake torque=0.

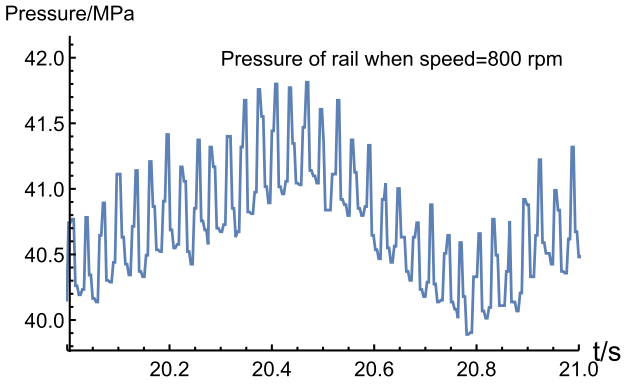

FIGURE 23. Experimental result of rail pressure when speed=800 rpm and brake torque=0.

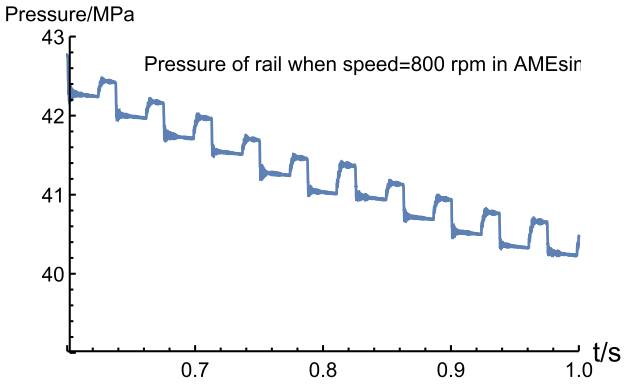

FIGURE 24. Experimental result of rail pressure when speed=2000 rpm and brake torque=0.

the experiment is obviously lower than the simulation result. This is because the rail pressure signal is read out from ECU, and the reading frequency cannot be too high otherwise it may interfere with the operation of ECU. Pressure fluctuations can also be measured with other sensors, as conducted in the literature [20]. However, such experimental conditions are not realistic for actual diesel engine products, though the measurement results of the literature are consistent with simulation results in this study.

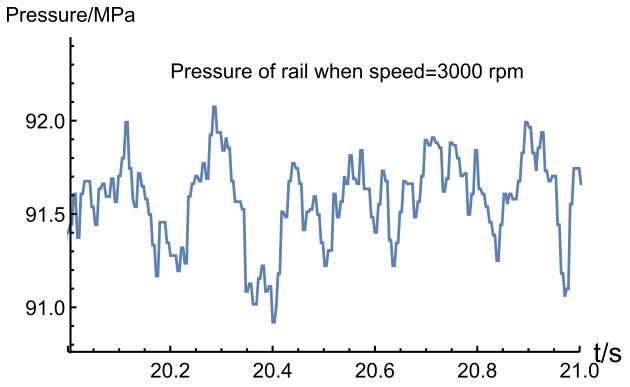

FIGURE 25. Experimental result of rail pressure when speed=3000 rpm and brake torque=0.

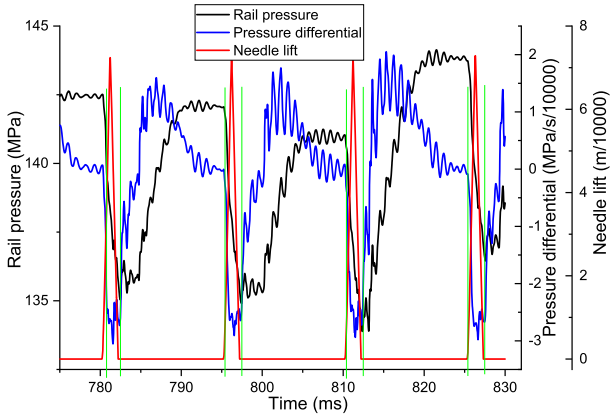

FIGURE 26. Needle lift and rail pressure with the SOI and EOI marked for engine speed=2000 rpm, brake torque=0 and target pressure=150 MPa.

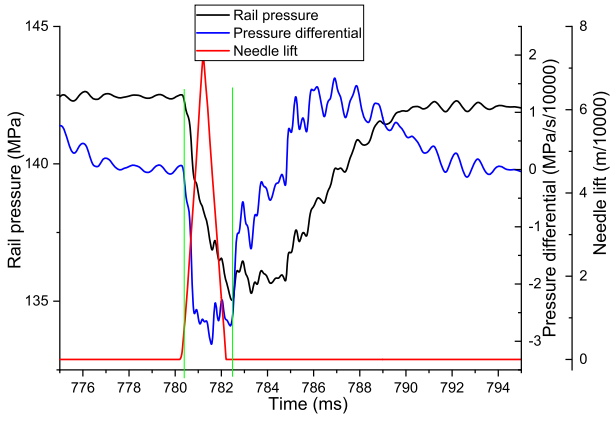

FIGURE 27. Single period enlarged plot of Fig. 26.

The rail pressure in RA420 SOHC is drawn for three typical speed cases being 800, 2000 and 3000 rpm, when brake torque is zero. This is displayed in Fig. 23-25. The sampling frequency in these results is not enough to highlight the details of pressure wave. However, when the experimental and simulation results are put together, they illustrate that pressure will lower after SOI and recover after EOI. Thus it

can be surmised that the simulation results can reveal details of the pressure wave. The simulation results are then used as the input for the signal processing algorithm.

The result of signal processing are displayed in Fig. 26-Fig. 27. In these figures, SOI and EOI are marked. This information, combined with the control algorithm injection starting or ending point, will provide the SOI and EOI. This can then be tabled as a MAP and stored in ECU, so the SOI and EOI can be closed-loop controlled.

VI. CONCLUSIONS

The importance of FIT and FIV in CRIS, as well as the current progress of research in this field was discussed in this paper. The working principle of solenoid valve injector was described, pressure wave propagation analyzed, and the characteristics of pressure waves were studied by simulation and experiments. It was found that pressure waves can be used as an imprint to draw the information of FIT.

This paper proposed innovative rail pressure sensor signal processing algorithms to determine the SOI and EOI, thereby enabling closed-loop control of the SOI, EOI and injection advance angle. The algorithm adopts the signal processing method to calculate the SOI and EOI and was found to have high reliability and flexibility as well as the ability to be adjusted in real time according to engine operating status. This method also has a high degree of integration and can be widely used in diesel engines with CRIS. The hardware implementation of this algorithm in practical ECU was also provided.

The algorithm can reduce the precision, tolerance and consistency of injector production, and can compensate the discrete characteristic of the fuel injection system. It can effectively avoid the defects and shortcomings of traditional engine matching calibration, and improve the control precision of the FIT and FIV. Thus, the proposed method can improve the consistency and stability of fuel injection and is expected to promote the performance of engine on fuel economy and pollutant emissions. The algorithm only needs to add corresponding modules to the engine's control system. Previous approaches [13], [15], change the structure of fuel injection system or engine. The proposed algorithm does not make the above changes, and it can be applied on existing engines, thus it has technical advantages.

As described above, the proposed algorithm does not depend on the fuel mass of each injection. For small injection mass, a high-precision rail pressure sensor is needed to measure the small change of rail pressure, so the algorithm can be used in multiple injections of CRIS in diesel engines. This algorithm has implications for injection system of gasoline engine. The corresponding control algorithm can be designed according to the pressure variation characteristics of the gasoline engine injection system.

REFERENCES

[1] D. Schiefer, R. Maennel, and W. Nardoni, "Advantages of diesel engine control using in-cylinder pressure information for closed loop control," SAE Tech. Paper 2003-01-0364, 2003.
[2] N. B. Jones and Y.-H. Li, "A review of condition monitoring and fault diagnosis for diesel engines," *Lubrication Sci.*, vol. 6, no. 3, pp. 267–291, 2000.
[3] J. A. Bittle, B. M. Knight, and T. J. Jacobs, "The impact of biodiesel on injection timing and pulsewidth in a common-rail medium-duty diesel engine," *SAE Int. J. Engines*, vol. 2, no. 2, pp. 312–325, 2009.
[4] S. Moon, Y. Matsumoto, and K. Nishida, "Entrainment, evaporation and mixing characteristics of diesel sprays around end-of-injection," SAE Tech. Paper 2009-01-0849, 2009.
[5] B. Knox and C. Genzale, "Effects of end-of-injection transients on combustion recession in diesel sprays," *SAE Int. J. Engines*, vol. 9, no. 2, pp. 932–949, 2016.
[6] E. S. Guerry, M. S. Raihan, K. K. Srinivasan, S. R. Krishnan, and A. Sohail, "Injection timing effects on partially premixed diesel–methane dual fuel low temperature combustion," *Appl. Energy*, vol. 162, pp. 99–113, Jan. 2016.
[7] M. Battistoni, C. Poggiani, and S. Som, "Prediction of the nozzle flow and jet characteristics at start and end of injection: Transient behaviors," *SAE Int. J. Engines*, vol. 9, no. 1, pp. 84–97, 2016.
[8] L. Chen, L. Liu, F. Yang, J. Li, K. Zhang, and M. Ouyang, "Diesel fuel system solenoid closure start-point and feedback control strategy," *Chin. J. Mech. Eng.*, vol. 46, no. 18, p. 025, 2010.
[9] Z. Y.-T. Li Pi-mao, "Influence of eddy current on transient characteristics of common rail injector solenoid valve," *J. Beijing Inst. Technol.*, vol. 24, no. 1, pp. 26–34, 2015.
[10] M. S. Ziemacki and G. D. Wolff, "Digital self-calibrating hall-effect sensor for electronically controlled engines," SAE Tech. Papers 860143, 1986.
[11] M. Ikemoto, K. Omae, K. Nishida, F. Arikawa, M. Oyama, and T. Tomoda, "In-cylinder experimental analysis using piezo-driven diesel injector equipped with needle-lift sensor," *JSAE Trans.*, vol. 41, no. 6, pp. 1347–1352, 2010.
[12] F. Estefanous and N. Henein, "Multi sensing fuel injector for electronically controlled diesel engines," SAE Tech. Paper 2011-01-0936, 2011.
[13] S. Rehman, "Sensors based measurement techniques of fuel injection and ignition characteristics of diesel sprays in di combustion system," *Alexandria Eng. J.*, vol. 55, no. 3, pp. 2391–2403, 2016.
[14] A. Kastengren *et al.*, "Correlation of split-injection needle lift and spray structure," SAE Tech. Papers 2011-01-0383, 2011.
[15] C. Crua and M. R. Heikal, "Time-resolved fuel injector flow characterisation based on 3d laser doppler vibrometry," *Meas. Sci. Technol.*, vol. 25, no. 12, p. 125301, 2014.
[16] K. Reif, *Diesel Engine Management: Systems and Components*. Wiesbaden, Germany: Springer Vieweg, 2014.
[17] Z. Reif, "High pressure common rail injector problem analysis," *Adv. Eng.*, vol. 3, no. 1, pp. 103–116, 2009.
[18] A. E. Catania, A. Ferrari, and E. Spessa, "Numerical-experimental study and solutions to reduce the dwell time threshold for fusion-free consecutive injections in a multijet solenoid-type CR system," in *Proc. ASME Internal Combustion Engine Divis. Spring Tech. Conf.*, 2006, pp. 317–332.
[19] F. Payri, J. Lujan, C. Guardiola, and G. Rizzoni, "Injection diagnosis through common-rail pressure measurement," *Proc. Inst. Mech. Eng., D, J. Automobile Eng.*, vol. 220, no. 3, pp. 347–357, 2006.
[20] T. Krogerus, M. Hyvönen, and K. Huhtala, "Analysis of common rail pressure signal of dual-fuel large industrial engine for identification of injection duration of pilot diesel injectors," *Fuel*, vol. 216, pp. 1–9, Mar. 2018.
[21] J.-J. Shu, "Modelling vaporous cavitation on fluid transients," *Int. J. Pressure Vessels Piping*, vol. 80, no. 3, pp. 187–195, 2003.
[22] V. K. Gupta, Z. Zhang, and Z. Sun, "Modeling and control of a novel pressure regulation mechanism for common rail fuel injection systems," *Appl. Math. Model.*, vol. 35, no. 7, pp. 3473–3483, 2011.
[23] A. E. Catania, A. Ferrari, and M. Manno, "Development and application of a complete multijet common-rail injection-system mathematical model for hydrodynamic analysis and diagnostics," *J. Eng. Gas Turbines Power*, vol. 130, no. 6, p. 062809, 2008.
[24] V. Amoia, A. Ficarella, D. Laforgia, S. De Matthaeis, and C. Genco, "A theoretical code to simulate the behavior of an electro-injector for diesel engines and parametric analysis," SAE Tech. Paper 970349, 1997.
[25] L. A. Catalano, V. Tondolo, and A. Dadone, "Dynamic rise of pressure in the common-rail fuel injection system," SAE Tech. Paper 2002-01-0210, 2002.
[26] K. M. Khan, *Fluid Mechanics and Machinery*. London, U.K.: Oxford Univ. Press, 2015.

[27] B. D. Nikolić, B. Kegl, S. D. Marković, and M. S. Mitrović, "Determining the speed of sound, density and bulk modulus of rapeseed oil, biodiesel and diesel fuel," *Thermal Sci.*, vol. 16, no. 2, pp. 505–514, 2012.
[28] S. Ball and J. Trusler, "Speed of sound of n-hexane and n-hexadecane at temperatures between 298 and 373 k and pressures up to 100 MPa," *Int. J. Thermophys.*, vol. 22, no. 2, pp. 427–443, 2001.
[29] C. Arcoumanis and R. J. Fairbrother, "Computer simulation of fuel injection systems for DI diesel engines," *SAE Trans.*, vol. 101, no. 3, pp. 1881–1898, 1992.

QINMIAO KANG was born in Xuchang, Henan Province, China, in 1987. He received the B.S. degree from the Tianjin University of Technology in 2012 and the M.S. degree from Tsinghua University, Beijing, China, where he is currently pursuing the Ph.D. degree with the School of Aerospace Engineering.

His research interests include wireless communication networks, wireless transmitter and receiver design, analog integrated circuit design, heavy oil helicopter control, and diesel engine control.

ZHIFENG XIE was born in Yili, Xijiang, China, in 1982. He received the M.S. degree from Zhejiang University in 2005 and the Ph.D. degree in theoretical physics from the Chinese Academy of Sciences in 2010. Since 2010, he has been a Research Assistant with the School of Aerospace Engineering, Tsinghua University, Beijing, China. His research interests mainly include the design of aeroengine, structural dynamics, fluid mechanism, vibration control, and engine electronic control.

YONG LI (M'09–SM'16) received the B.S. degree in electronics and information engineering from the Huazhong University of Science and Technology, Wuhan, China, in 2007, and the Ph.D. degree in electronic engineering from Tsinghua University, Beijing, China, in 2012. He is currently a Faculty Member with the Department of Electronic Engineering, Tsinghua University.

Dr. Li has served as the general chair, the TPC chair, and a TPC member for several international workshops and conferences, and he is on the editorial board of three international journals. His papers have total citations of more than 2300 (six papers exceed 100 citations, Google Scholar). Among them, eight are ESI Highly Cited Papers in computer science, and four received conference best paper (run-up) awards. He received the IEEE 2016 ComSoc Asia-Pacific Outstanding Young Researchers and the Young Talent Program of China Association for Science and Technology.

YONGQUAN LIU was born in 1963. He received the B.S. degree in aeroengine design from Northwestern Polytechnical University in 1984, and the M.S. and Ph.D. degrees from Beihang University. He is currently a Researcher and Doctoral Tutor of the 606 Institute, Chinese Aeronautical Establishment.

His research interests include turbine engine design, rotor dynamics, advanced technology and informatization of aircraft engines, overall design and planning of aeroengine, structural strength and vibration, mechanical dynamics, and machine vibration diagnosis and control.

MING ZHOU was born in 1962. He received the B.S. degree from Northwestern Polytechnical University in 1984, the M.S. and Ph.D. degrees from Beihang University in 1993 and 1996, respectively, and the Post-Doctoral degree in power engineering and control from Tsinghua University, Beijing, China. He is currently a Professor with the School of Aerospace Engineering, Tsinghua University. His research interests include diesel engine design, engine control, rotor-bearings dynamics, and fuel injection system design.